

# Learning to Generate Text-grounded Mask for Open-world Semantic Segmentation from Only Image-Text Pairs

Junbum Cha

Jonghwan Mun

Byungseok Roh

Kakao Brain

{junbum.cha, jason.mun, peter.roh}@kakaobrain.com

## Abstract

We tackle open-world semantic segmentation, which aims at learning to segment arbitrary visual concepts in images, by using only image-text pairs without dense annotations. Existing open-world segmentation methods have shown impressive advances by employing contrastive learning (CL) to learn diverse visual concepts and adapting the learned image-level understanding to the segmentation task. However, these methods based on CL have a discrepancy since it only considers image-text level alignment in training time, while the segmentation task requires region-text level alignment at test time. In this paper, we propose a novel **Text-grounded Contrastive Learning (TCL)** framework to directly align a text and a region described by the text to address the train-test discrepancy. Our method generates a segmentation mask associated with a given text, extracts grounded image embedding from the masked region, and aligns it with text embedding via TCL. The framework addresses the discrepancy by letting the model learn region-text level alignment instead of image-text level alignment and encourages the model to directly improve the quality of generated segmentation masks. In addition, for a rigorous and fair comparison, we present a unified evaluation protocol with widely used 8 semantic segmentation datasets. TCL achieves the state-of-the-art zero-shot segmentation performances with large margins in all datasets. Code is available at <https://github.com/kakaobrain/tcl>.

## 1. Introduction

Open-world semantic segmentation aims to identify the arbitrary semantic concepts in the open world<sup>1</sup>. Conventional semantic segmentation aims to learn segmentation capability for the small number of pre-defined target categories, whereas open-world semantic segmentation ad-

<sup>1</sup>This setting is often called both *open-world* and *open-vocabulary*. In this paper, we mainly refer to this setting as *open-world* for clarity.

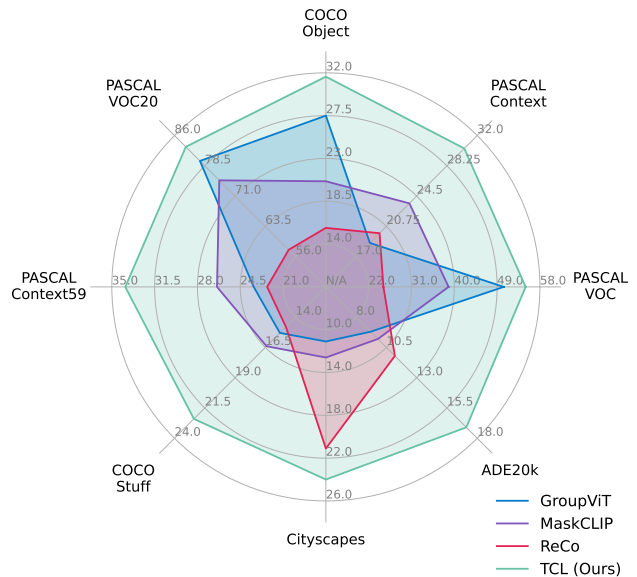


Figure 1. **Open-world segmentation performance comparison.** The proposed method remarkably outperforms existing methods in all 8 segmentation benchmark datasets.

resses unrestricted arbitrary categories or free-form texts. Such segmentation capability over unlimited targets drastically extends the application scope of the open-world segmentation model.

The first challenge for open-world segmentation is how to learn arbitrary concepts, not pre-defined categories. Inspired by the success of CLIP [24], previous approaches [11, 18–20, 29, 31, 34] tackle this challenge by exploiting massive web-crawled image-text paired data; since the texts in web-crawled data contain a global semantic description for the paired images, the large-scale image-text pairs can provide rich knowledge for arbitrary semantic categories. However, there still remains another challenge in how to achieve precise localization of arbitrary concepts without dense annotations. There are several approaches that simply address this issue using dense annotation (seg-

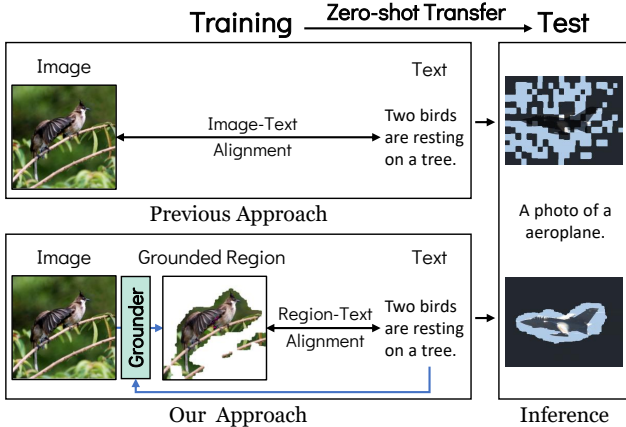


Figure 2. **A conceptual comparison between the previous approach and ours.** Open-world segmentation is typically achieved by matching region features and text embeddings. However, previous methods learn image-level alignment during training, thus suffering from the alignment-level discrepancy between training and test. In contrast, our method lets the model learn region-text alignment with only image-text data in an end-to-end manner.

mentation masks) in addition to image-text pairs [11, 18, 19]. The dense annotation helps to improve segmentation performance in a fixed benchmark dataset, but the requirements of expensive dense annotation still limit the applicable domains and scalability of the method.

In this paper, therefore, we focus on open-world semantic segmentation from only image-text pairs without any dense annotation. For the setting, the existing methods [20, 29, 31, 34] mainly rely on the transferability of the image-text alignment capability learned during the training to perform region-text alignment at inference time. More specifically, MaskCLIP [34] leverages a pre-trained model such as CLIP, simply modifies its last layer to extract more precise patch-level visual features, and finally generates segmentation masks by patch-text matching. GroupViT [31] and ViL-Seg [20] propose to cluster region-level visual features into distinct groups and generate segmentation masks by matching the groups and texts. Note that they match the text embeddings and clustered region features in test time, but in training time, the text embeddings are aligned with global image embeddings. While the existing methods have shown impressive results even from the training with image-text alignment, they still suffer from the alignment-level discrepancy between training and test as depicted in Fig. 2. This training-test discrepancy in the alignment can weaken open-world segmentation capability.

To tackle such limitation, we propose the **Text-grounded Contrastive Learning (TCL)** framework, which addresses the training-test discrepancy issue by directly learning to align text and region of interest from the image-text data. Our key idea is to incorporate a text grounding procedure within contrastive learning as shown in Fig. 2. To

be specific, given a pair of image and text, we first obtain a segmentation mask indicating text-grounded regions using a grounder, compute grounded region embeddings using the segmentation mask, and finally apply contrastive learning between the text and the grounded region. By reformulating the contrastive loss to be directly affected by the segmentation quality, TCL enables to train the grounder and directly improves the quality of text-region level alignment in an end-to-end manner. In addition, we present a unified evaluation protocol with widely used 8 semantic segmentation datasets and compare existing methods in the same setting using the protocol. TCL achieves state-of-the-art zero-shot segmentation performance with large margins in all datasets as shown in Fig. 1.

Our main contributions are summarized as follows:

- We introduce a novel framework for open-world semantic segmentation, named Text-grounded Contrastive Learning, which directly optimizes alignment between text and region of interest without train-test discrepancy, thus learning to generate more precise segmentation masks even from only image-text pairs.
- We present a unified evaluation protocol and re-evaluate recent open-world segmentation models for a fair and direct comparison.
- We achieve the new state-of-the-art zero-shot segmentation performance on 8 segmentation datasets with large margins compared to existing methods.

## 2. Related Works

### 2.1. Open-world Semantic Segmentation

**Open-world** scenario aims to recognize arbitrary concepts in the open world. It is also called **open-vocabulary** because the target vocabulary is open rather than closed. Contrastive Language-Image Pre-training (CLIP) [24] ushered in the era of open-world image recognition using large-scale image-text pairs [2, 5, 27, 28]. CLIP learns the alignment between an image and a text in training time, then transfer it to the zero-shot classification by aligning image and texts indicating target classes at inference time. The advent of CLIP enables open-world settings in various fields such as object detection [13, 32], image captioning [14], or semantic segmentation [31, 34].

**Open-world semantic segmentation with image-text pairs** is addressed in two different settings. The first is a **semi-supervised setting**, which uses dense annotation (*i.e.*, segmentation masks) in addition to image-text pairs [11, 18, 19]. Semi-supervised approaches learn segmentation capability using dense annotation and expand the target vocabulary using image-text supervision. LSeg [18] expands target class vocabulary using image-label datasets and CLIP text encoder [24]. OpenSeg [11] and OVSeg [19] first train a mask generator using dense annotation and

expand target vocabulary using image-text datasets. The use of dense annotation makes the model learn region-level alignment instead of image-level alignment, leading to high-quality segmentation masks. However, it still relies on costly dense annotation, and applicable domains are limited to the domains where dense annotation is available.

The target of this paper is an **unsupervised setting**, which aims to learn segmentation from only image-text pairs without any dense annotation [20, 29, 31, 34]. Since the massive image-text pairs are easily obtained by web crawling without human annotators, applicable domains of unsupervised methods become almost unlimited. In order to achieve segmentation capability using only image-text pairs, we need to learn region-text alignment instead of image-text alignment and train a text-grounded mask generator. However, the absence of dense annotation makes this approach challenging. Existing open-world semantic segmentation studies have taken a strategy to bypass this issue. Instead of learning region-level alignment directly, they transfer image-level alignment to region-level by heuristic modification [29, 34] or clustering [20, 31]. MaskCLIP [34] proposes to obtain a dense image embedding from CLIP image encoder through heuristic modification of the last attention layer. Even though it has several limitations, such as low output resolution or noisy segmentation results, they show it is a simple yet effective way to obtain an initial segmentation map for refinement. ReCo [29] proposes an advanced refinement method based on MaskCLIP, by retrieval and co-segmentation. Clustering-based methods [20, 31] learn representations using CL with image-text pairs. They compute region-level image embedding by clustering sub-region embeddings. These approaches also have shown impressive results but have several limitations: (i) the learning objective is still image-level alignment due to lack of the region annotation, (ii) the number of clusters is pre-defined independent of the given image, and (iii) clustering sub-region image embeddings is independent of the query text. In summary, existing methods indirectly address region-level alignment problems by learning image-level alignment. To tackle this problem, we propose a novel region-level alignment objective, named Text-grounded Contrastive Learning (TCL).

## 2.2. Region-level Contrastive Learning

Learning region-level alignment instead of image-level alignment is a fundamental target objective in dense tasks, such as segmentation or object detection. There are approaches to learn region-level alignment using dense annotation in the semi-supervised setting. They first train mask or region proposal networks using dense annotation and learn alignment between the proposals and texts [11, 16, 32]. For example, OpenSeg [11] trains a class-agnostic mask generator using dense annotation. In the object detection

field, RegionCLIP [32] employs an off-the-shelf region proposal network and learns region-level alignment. In contrast to the existing region-level methods, the proposed method learns region-level alignment without any dense annotation.

## 3. Methods

### 3.1. Overview

Open-world semantic segmentation is a task that aims to learn a model having zero-shot segmentation capability for arbitrary visual concepts, not restricted to pre-defined ones. Our main goal is to develop an open-world segmentation algorithm using image-text paired data only. This objective is hard to achieve particularly because there is no explicit supervision (*i.e.*, pixel-level dense annotations) for the segmentation of the text-described region. Therefore, for a random image and text pair  $(\mathbf{x}^V, \mathbf{x}^T)$ , existing methods typically learn models parametrized by  $\theta$  to maximize the mutual information between paired images and texts [23, 24] as follows:

$$\arg \max_{\theta} I_{\theta}(\mathbf{x}^V; \mathbf{x}^T). \quad (1)$$

This objective encourages the model to learn the alignment between texts and images, however, at inference time, the learned model requires generating segmentation masks for texts of arbitrary visual concepts by computing region-text alignments. Such alignment-level discrepancy between training and inference time may lead the model to a sub-optimal solution as shown in Fig. 2. With this in consideration, to bridge the gap between the objective of conventional contrastive learning and the requirement in the segmentation process, we propose Text-grounded Contrastive Learning (TCL) which incorporates a text grounding process to directly align text and regions of interest; for the text grounding, we introduce a grounder that is in charge of generating segmentation masks for the given texts. In a nutshell, TCL learns a model to maximize mutual information between texts and text-grounded regions as follows:

$$\arg \max_{\theta} I_{\theta}(\mathbf{m} \cdot \mathbf{x}^V; \mathbf{x}^T), \quad (2)$$

where  $\mathbf{m}$  is a text-grounded mask of random variable indicating the regions described by a given text. Compared to contrastive learning that implicitly learns a grounding capability, TCL has a clear advantage of explicitly learning the grounding capability from the end-to-end trainable grounder.

In the rest of this section, we first explain the text-grounded mask generation procedure by the grounder. Then, we describe how we define losses using the generated mask to train our open-world grounder with text-grounded contrastive learning. Finally, we explain how our model performs zero-shot inference for arbitrary concepts.

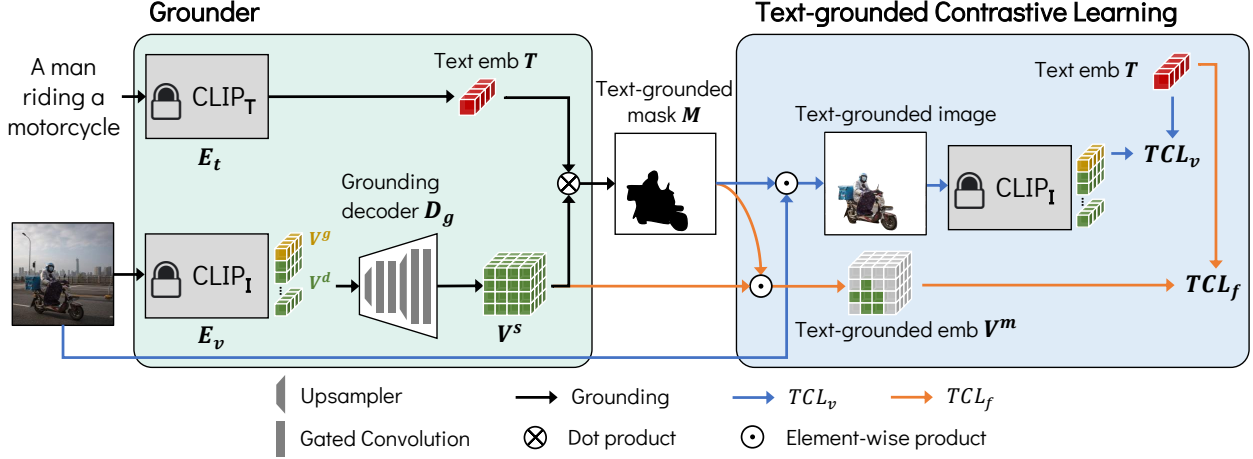


Figure 3. **Overall training pipeline of TCL.** The proposed TCL framework first obtains text-grounded masks using a grounder and then learns the grounder using text-grounded contrastive learning. By incorporating the text grounding process with contrastive learning, our framework can directly learn region-text alignment that is required for precise segmentation.  $\text{CLIP}_T$  and  $\text{CLIP}_I$  indicate CLIP text and image encoders, respectively. CLIP encoders are frozen and we train the grounding decoder only. After training, the TCL block is discarded, and only the Grounder block is used to generate the text-grounded segmentation mask for inference.

### 3.2. Grounder

Fig. 3 illustrates our overall training pipeline. For an input batch of paired texts  $\mathbf{X}^T$  and images  $\mathbf{X}^V$ , TCL first performs a grounding process to identify text-grounded regions for a text via a grounder. The grounder consists of three components: (i) image encoder  $E_v$  is in charge of providing a single (L2-normalized) global feature as well as dense patch-level features, (ii) text encoder  $E_t$  provides a (L2-normalized) text embedding feature, and (iii) grounding decoder  $D_g$  converts dense features from image encoder into finer pixel-level embeddings for alignment with text. In practice, as shown in Fig. 3, we adopt CLIP [24] to initialize two encoders. To preserve and exploit the rich knowledge of CLIP learned during large-scale pre-training, we freeze the pre-trained CLIP. The text-grounded masks are computed by position-wise dot product between text embedding and dense pixel-level embedding. The overall process of grounder is summarized as follows:

$$\mathbf{T} = E_t(\mathbf{X}^T) \quad \text{and} \quad \mathbf{V}^g, \mathbf{V}^d = E_v(\mathbf{X}^V), \quad (3)$$

$$\mathbf{V}^s = D_g(\mathbf{V}^d), \quad (4)$$

$$\mathbf{M}_{i,j} = \sigma(w \cdot \mathbf{t}_j^\top \mathbf{V}_i^s + b), \quad (5)$$

where  $\mathbf{T} \in \mathbb{R}^{B \times C}$ ,  $\mathbf{V}^g \in \mathbb{R}^{B \times C}$ , and  $\mathbf{V}^d \in \mathbb{R}^{B \times L \times C}$  are a normalized text embedding, a normalized global image embedding, and dense image features from CLIP encoders,  $\mathbf{V}^s \in \mathbb{R}^{B \times C \times H \times W}$  is a normalized pixel-level dense embedding by the grounding decoder, and  $\mathbf{M} \in \mathbb{R}^{B \times B \times H \times W}$  is text-grounded masks between images and texts in the batch.  $B$ ,  $C$ , and  $L$  indicate a batch size, the embedding dimension size, and the number of patches, respectively.  $\sigma$  is a sigmoid function, and  $w, b$  are learnable parameters for

scalar projection.

The generated text-grounded masks are used to extract text-grounded image embedding. By replacing the global image embedding with text-grounded image embedding in the contrastive learning framework, TCL makes the model learn text-region level alignment in an end-to-end manner. In the following section, we describe how the generated mask  $\mathbf{M}$  is used for text-grounded contrastive learning.

### 3.3. Text-grounded Contrastive Learning

Recall that the main idea of TCL is to define positive pairs for contrastive learning as grounded regions and texts. For this purpose, we define TCL losses in two different levels—image-level and feature-level—using the generated masks  $\mathbf{M}$  for all pairs of images and texts in a batch; the detailed pseudo code to compute TCL losses is in Appendix B. In addition, we employ area prior loss and smooth prior loss to further improve the quality of generated masks.

**Image-level TCL loss.** Given a pair of image  $\mathbf{X}_i^V$  and text  $\mathbf{X}_i^T$ , one intuitive way to obtain a feature for grounded regions is directly inferring a masked image given by a generated segmentation mask. To make the whole process end-to-end trainable, we first compute a binarized mask  $\mathbf{M}_{i,i}^b$  from the generated mask  $\mathbf{M}_{i,i}$  using Gumbel-Max [15] technique and obtain a differentiable masked image via element-wise multiplication of the given image and the binarized mask. Then, we feed the masked image into the image encoder,  $\tilde{\mathbf{v}}_i^g, \tilde{\mathbf{v}}_i^d = E_v(\mathbf{M}_{i,i}^b \cdot \mathbf{X}_i^V)$ , and use the extracted global vector  $\tilde{\mathbf{v}}_i^g$  as the text-grounded image embedding. We compute a cosine similarity matrix between text-grounded image embeddings and text embeddings in a batch by  $S_{i,j}^m =$



$\tilde{\mathbf{v}}_i^g \top \mathbf{t}_j$ . Finally, based on the similarity matrix, we define the image-level TCL loss  $\mathcal{L}_{\text{TCL}_v}$  to make the representations of positive image-text pairs similar to each other while the representations of negative pairs dissimilar using the symmetric version of InfoNCE [23, 24]:

$$\mathcal{L}_{\text{TCL}_v} = \text{InfoNCE}(\mathbf{S}^m), \quad (6)$$

$$\begin{aligned} \text{InfoNCE}(\mathbf{S}) = & -\frac{1}{2B} \sum_i^B \log \frac{\exp(S_{i,i}/\tau)}{\sum_j^B \exp(S_{i,j}/\tau)} \\ & -\frac{1}{2B} \sum_i^B \log \frac{\exp(S_{i,i}/\tau)}{\sum_j^B \exp(S_{j,i}/\tau)}, \end{aligned} \quad (7)$$

where  $\tau$  is a learnable temperature.

**Feature-level TCL loss.** While the image-level TCL loss drives a model to generate segmentation masks for the associated texts (*i.e.*, text of positive pairs in the batch), we observe that it is not enough to suppress a segmentation mask for the region that is not described in the text, especially for the salient region. This raises the need to optimize negative masks obtained from the unrelated text (*i.e.*, the text of negative pairs in the batch). However, it is infeasible to compute the image-level TCL loss for negative masks due to the high computational cost of inferring grounded image embeddings. Motivated by [12], we introduce the feature-level TCL loss to effectively compute features of the negative masks. Specifically, for pixel-level dense embeddings  $\mathbf{V}_i^s \in \mathbb{R}^{C \times H \times W}$  from grounding decoder and a text embedding vector  $\mathbf{t}_j$ , we compute feature-level grounded image embedding  $\mathbf{v}_{i,j}^f \in \mathbb{R}^C$  by:

$$\mathbf{v}_{i,j}^f = \frac{\sum_{h,w} M_{i,j,h,w} \cdot \mathbf{v}_{i,:h,w}^s}{\sum_{h,w} M_{i,j,h,w}}. \quad (8)$$

Then, we compute a cosine similarity  $S_{i,j}^f = \mathbf{v}_{i,j}^f \top \mathbf{t}_j$  between all pairs of text embeddings and feature-level text-grounded image embeddings in the batch. Finally, we define the feature-level TCL loss to suppress the grounding of negative texts using the similarity matrix as follows:

$$\mathcal{L}_{\text{TCL}_f} = \text{InfoNCE}(\mathbf{S}^f). \quad (9)$$

**Area prior loss.** When training with only TCL losses, the model can collapse into a trivial solution—generating text-grounded masks that capture the entire image instead of the exact text-described region. To prevent the collapse, we leverage priors about segmentation area into our TCL framework. To be specific, for the positive masks (masks from positive pairs)  $\mathbf{M}^+$  and the negative masks (masks from negative pair)  $\mathbf{M}^-$ , we denote the area of positive and

negative masks by  $\overline{\mathbf{M}}^+$  and  $\overline{\mathbf{M}}^-$ , respectively. The area prior loss is defined by L1-distance between a prior and each area:

$$\mathcal{L}_{\text{area}} = \left\| p^+ - \mathbb{E}[\overline{\mathbf{M}}^+] \right\|_1 + \left\| p^- - \mathbb{E}[\overline{\mathbf{M}}^-] \right\|_1, \quad (10)$$

where  $p^+$  and  $p^-$  are positive and negative area priors. For the negative area prior  $p^-$ , intuitively, we can expect the area of the negative masks to be 0.0. We set the positive area prior  $p^+$  to 0.4, which is the average text-described region area measured by MaskCLIP [34] in the CC3M dataset [28].

**Smooth prior loss.** In the image-text dataset, a text generally describes the salient object or semantic in the paired image. Based on the observation, we assume that most of the text-described region is smooth rather than noisy (like including holes). We employ total variation (TV) regularization loss [25] for the smooth prior. We apply total variation loss to both mask and pixel-level dense embedding:

$$\mathcal{L}_{\text{tv}} = \|\mathbf{M}\|_{\text{TV}} + \|\mathbf{V}^s\|_{\text{TV}}, \quad (11)$$

where  $\|\cdot\|_{\text{TV}}$  is the anisotropic TV norm.

**Final loss.** Our final loss function is defined by:

$$\mathcal{L} = \lambda_{\text{TCL}} \mathcal{L}_{\text{TCL}} + \lambda_{\text{area}} \mathcal{L}_{\text{area}} + \lambda_{\text{tv}} \mathcal{L}_{\text{tv}}, \quad (12)$$

where  $\mathcal{L}_{\text{TCL}} = \mathcal{L}_{\text{TCL}_v} + \mathcal{L}_{\text{TCL}_f}$ , and  $\lambda_{\text{TCL}}$ ,  $\lambda_{\text{area}}$ ,  $\lambda_{\text{tv}}$  are hyperparameters to balance three losses.

### 3.4. Inference Pipeline

The zero-shot inference pipeline is almost the same as CLIP [24]. The only difference is that we conduct pixel-level classification instead of image-level classification. Specifically, for text embeddings  $\mathbf{T} \in \mathbb{R}^{N \times C}$  and a pixel-level dense embedding  $\mathbf{v}^s \in \mathbb{R}^{C \times H \times W}$ , text-grounded mask  $\mathbf{M} \in \mathbb{R}^{N \times H \times W}$  is computed by Eq. (5), where  $N$  is the number of target classes. The final segmentation map  $\mathcal{M}$  is computed by:

$$\mathcal{M}_{h,w} = \arg \max_i M_{i,h,w}, \quad (13)$$

where we use prompt templates to generate text embeddings following CLIP, *e.g.*, “a photo of a {label}.”.

## 4. Experiments

### 4.1. Experiment Settings

**Unified evaluation protocol.** In open-world semantic segmentation, a standard evaluation protocol is not yet established. Previous studies conduct an evaluation using their own protocols such as different data processing strategies on different datasets [20, 29, 31, 34]; surprisingly, even

Methods	with background class			without background class					Avg.
	VOC	Context	Object	VOC20	Context59	Stuff	City	ADE	
GroupViT (YFCC)	49.5	19.0	24.3	74.1	20.8	12.6	6.9	8.7	27.0
GroupViT (RedCaps)	<u>50.4</u>	18.7	<u>27.5</u>	<u>79.7</u>	23.4	15.3	11.1	9.2	<u>29.4</u>
MaskCLIP <sup>†</sup>	29.3	21.1	15.5	53.7	23.3	14.7	<u>21.6</u>	10.8	23.7
MaskCLIP	38.8	<u>23.6</u>	20.6	74.9	<u>26.4</u>	<u>16.4</u>	12.6	9.8	27.9
ReCo	25.1	19.9	15.7	57.7	22.3	14.8	21.1	<u>11.2</u>	23.5
TCL (Ours)	<b>55.0</b>	<b>30.4</b>	<b>31.6</b>	<b>83.2</b>	<b>33.9</b>	<b>22.4</b>	<b>24.0</b>	<b>17.1</b>	<b>37.2</b>
	<b>(+4.6)</b>	<b>(+6.8)</b>	<b>(+4.1)</b>	<b>(+3.5)</b>	<b>(+7.5)</b>	<b>(+6.0)</b>	<b>(+2.4)</b>	<b>(+5.9)</b>	<b>(+7.8)</b>

Table 1. **Zero-shot segmentation performance comparison on 8 semantic segmentation datasets.** mIoU metric is used in every experiment. We highlight the best and second-best results. MaskCLIP<sup>†</sup> indicates their baseline method without additional refinement techniques. The YFCC and RedCaps of GroupViT indicate their training datasets in addition to CC12M. Each dataset abbreviation stands for VOC: PASCAL VOC, Context: PASCAL Context, Object: COCO-Object, Stuff: COCO-Stuff, City: Cityscapes, ADE: ADE20K.

for the same dataset, the target classes are sometimes different across studies. For a fair and direct comparison, we present a unified evaluation protocol. We design the protocol following the open-world scenario where prior access to the target data before evaluation is not allowed. Under this scenario, the proposed protocol prohibits dataset-specific hyperparameters or tricks, *e.g.*, class name expansion or rephrasing, leading to performance overestimation. For example, we observe that TCL can get significant performance gains by expanding the target class of “person” to its sub-concepts (*e.g.*, man, woman, worker, rider, etc.), but the kinds of class name-based tricks are not allowed in our unified evaluation protocol because the expansion depends on the target class names. With this consideration, we evaluate models using unified class names from the default version of MMSegmentation [8] without class name-based tricks. In addition, dense CRF [17] is not used identically due to its expensive computational cost. All other evaluation settings follow GroupViT [31], where the input image is resized to have a shorter side of 448. We employ mean intersection-over-union (mIoU) as a performance metric, which is a standard metric in semantic segmentation.

**Benchmark datasets and comparison methods.** To provide an extensive evaluation, we first collect all previously used benchmark datasets in the existing methods and add widely used ADE20K dataset for segmentation, resulting in a total of 8 benchmark datasets—categorized into 2 groups: (i) w/ background class: PASCAL VOC (21 classes), PASCAL Context (60 classes), COCO-Object (81 classes) [31] and (ii) w/o background class: PASCAL VOC20 (20 classes) [10], PASCAL Context59 (59 classes) [22], COCO-Stuff (171 classes) [3], Cityscapes (19 classes) [9], and ADE20K (150 classes) [33]. Note that open-world segmentation methods perform segmentation based on the text embedding of a class name. Thus, the background class, which does not sufficiently describe the semantic itself, needs additional considerations, *e.g.*,

probability thresholding instead of using the text embedding of “background” text. The datasets with background class evaluate this aspect. We compare TCL with all existing open-sourced methods: GroupViT [31], MaskCLIP [34], and ReCo [29] under the unified protocol. We also include their variants in comparison baselines for an extensive comparison. Additional details and comparisons with non-open-sourced methods are given in Appendix C.

**Implementation details.** For the grounder, we use the CLIP ViT-B/16 model where the size of input images is  $224 \times 224$  and the patch size is  $16 \times 16$ . Following MaskCLIP [34], we modify the last attention layer of the CLIP image encoder to acquire the dense embedding representing local semantics. The grounding decoder consists of four gated convolution blocks with two upsampling interpolations, where the output of a convolution block is gated by a learned gating parameter and added to the skip connection. We adopt pixel-adaptive mask refinement (PAMR) [1] for mask refinement. A detailed description of the model architecture is given in Appendix A. We use CC 3M and 12M datasets [5, 28] for training. The loss weights of  $\lambda_{\text{TCL}} = 0.1$ ,  $\lambda_{\text{area}} = 0.4$ ,  $\lambda_{\text{tv}} = 1.0$  are used. We train a model with a batch size of 1024 and a learning rate of  $7.5 \times 10^{-5}$  for total 50,000 iterations with 15,000 warmup steps and cosine schedule. AdamW optimizer [21] is used with a weight decay of 0.05.

## 4.2. Zero-shot Transfer to Semantic Segmentation

In Table 1, we first extensively compare all of the existing open-world semantic segmentation methods based on the proposed unified protocol, including two checkpoints of GroupViT [31] and two variants of MaskCLIP [34]. Between the existing methods, GroupViT achieves the best on average, but the best method varies according to each dataset. Interestingly, GroupViT shows the best performance on the object-oriented datasets (VOC, VOC20, and COCO-Object), but the performance tends to decrease as

the stuff classes are dominated in the target dataset. For example, GroupViT (RedCaps) presents the worst or second-worst performance in Context, Cityscapes, and ADE20K. In contrast, MaskCLIP shows the best performance in stuff-oriented datasets such as Context, Context59, and COCO-Stuff. We conjecture it benefits from leveraging a large-scale pre-trained CLIP model. Furthermore, their refinement techniques (key smoothing and prompt denoising) improve the average performance by +4.2 mIoU, but significantly degrade the performance in Cityscapes (21.6  $\rightarrow$  12.6). It may suggest a limitation of the heuristic refinement and the need for a data-driven approach. The significant performance degradation of MaskCLIP and ReCo between VOC20 and VOC (74.9  $\rightarrow$  38.8 and 57.7  $\rightarrow$  25.1) may imply the need for consideration for background class.

Even though the performance gap varies according to the characteristics of the evaluation dataset, TCL achieves the best performances with large margins in all datasets. These results support that our TCL framework successfully eliminates the train-test discrepancy in the alignment level existing in the previous methods and learns the region-level alignment. In addition, region-level alignment learning of TCL lets our model learn the capability to distinguish the background region in a data-driven manner, thus, our method can address the background class without any heuristic post-processing that the previous methods typically rely on.

### 4.3. Qualitative Results

**Visualization of the generated text-grounded masks.** Fig. 4 illustrates the impact of incorporating the grounding decoder. Since we follow MaskCLIP [34] modification, the results in “w/o  $D_g$ ” rows can be regarded as the initial results of MaskCLIP before refinement. Despite the vast pre-training scale and remarkable zero-shot classification performance of CLIP [24], its grounding capability is limited because the learning objective targets image-level alignment (See “w/o  $D_g$ ” rows). In contrast, the grounding decoder ( $D_g$ ) learns the region-level alignment by TCL, resulting in more accurate, finer, and less noisy generated masks (See “w/  $D_g$ ” rows).

**Qualitative comparison.** We compare the proposed method qualitatively in Fig. 5. At qualitative examples on the PASCAL VOC dataset Fig. 5a, we observe various types of errors in each comparison method. The grouping procedure of GroupViT [31] makes the segmentation results less noisy, but it also causes a wrong segmentation of a large group. ReCo [29] has difficulty in segmentation of background region due to the lack of consideration about the background class. MaskCLIP [34] does not take this into account as well, but its refinement methods make the results less noisy. In addition, we present examples in the

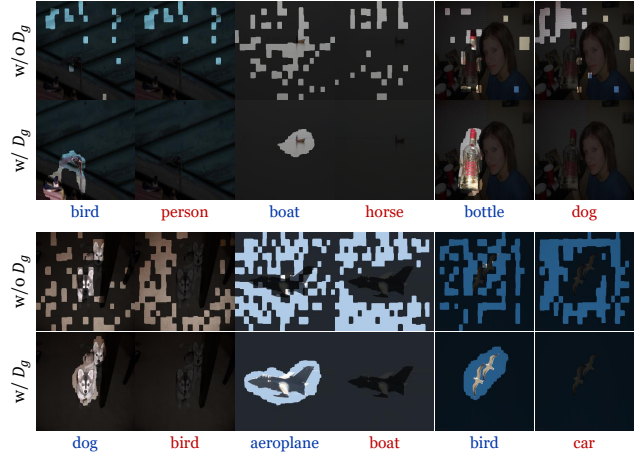


Figure 4. **Visualization of the generated text-grounded masks.** “w/o  $D_g$ ” rows show the generated text-grounded masks without the grounding decoder ( $D_g$ ), *i.e.*, CLIP dense features  $\mathbf{V}^d$  are used for alignment with texts instead of pixel-level dense embedding  $\mathbf{V}^s$ . “w/  $D_g$ ” rows show the results with the grounding decoder. For each image, we compare results for **positive** (blue) and **negative** (red) prompts shown below images. The results show that the grounder accurately and finely captures the text-described region with less noise via the grounding decoder.

wild to show open-world segmentation capability in Fig. 5b. We collect the image samples with visual concepts not included in conventional segmentation datasets (*e.g.*, moon, sunset) or free-form texts (*e.g.*, “two women and one man with a smiling snowman”). GroupViT tends to focus on the main object of the image and regard the other objects as background, which is consistent with its good performance in object-oriented datasets. Interestingly, in this qualitative comparison in the wild, we observe ReCo consistently outperforms MaskCLIP in contrast to the other results. We conjecture that this is due to their different refinement approaches; the refinement approach of ReCo is a data-driven method while the refinement approach of MaskCLIP depends on heuristic post-processing which does not guarantee general improvement. Compared with the baselines, TCL consistently generates the most precise segmentation masks. These results show that learning the region-level alignment by TCL improves the segmentation quality in both the evaluation dataset and web images in the wild. Additional qualitative results are provided in Appendix G.

### 4.4. Ablation Study

We investigate the contributions of individual loss terms by ablation studies on the PASCAL VOC20 and PASCAL Context59 datasets. We use a short learning schedule with a batch size of 512 for total 40,000 iterations including 10,000 warmup steps. Table 2a shows the influence of each component of the TCL loss, and how much the proposed TCL loss improves the segmentation performance

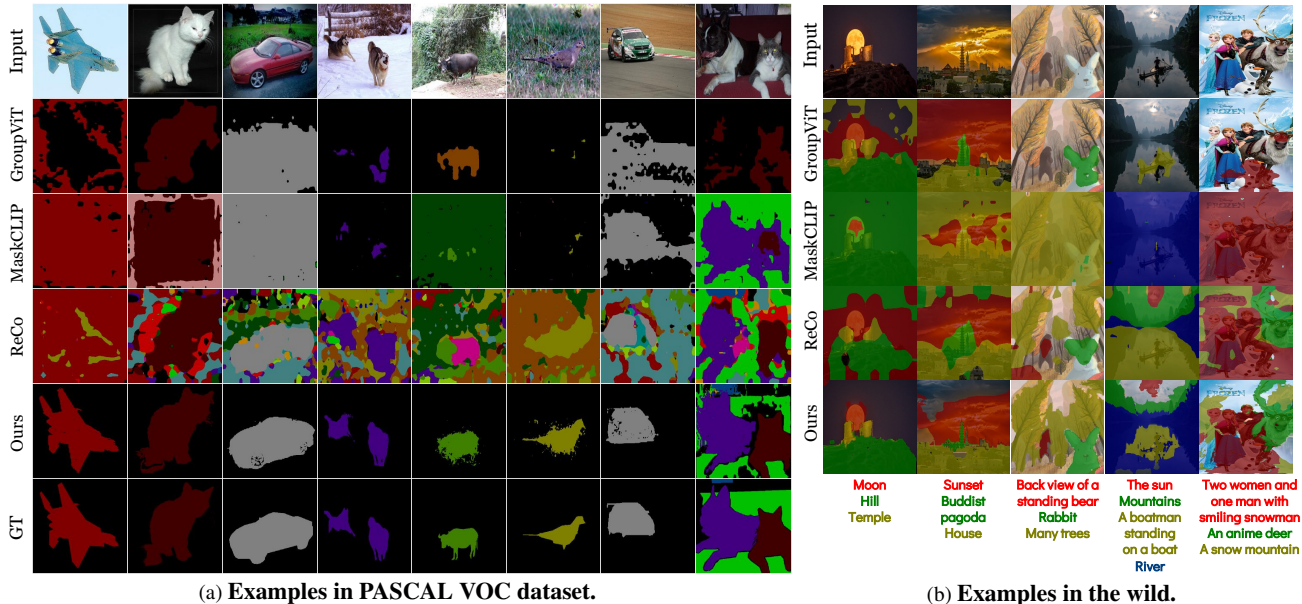


Figure 5. (a) The comparison shows the error types of each method in the VOC dataset. GroupViT tends to make an error on a large group rather than noisy results. ReCo suffers from segmentation of the background region. MaskCLIP tends to fail at capturing the target area precisely. (b) shows results on the wild web images and free-form texts. Texts used as target classes are shown at the bottom of the images.

compared to the conventional CL loss. In this setting with CL loss, the grounder is trained with the identical framework, but the learning objective is CL instead of TCL. We adopt attention pooling following CLIP [24] to compute global image embedding from the dense image embedding  $V^s$ . As shown in the table, the proposed TCL loss remarkably improves the segmentation performance in both VOC20 (69.7  $\rightarrow$  78.1) and Context59 (22.1  $\rightarrow$  29.1). Image-level or feature-level TCL loss solely improves the performance significantly, and using both losses together provides further performance gain. Also, we do not employ CL in addition to TCL (CL+TCL), since its mIoU varies depending on the dataset and average performance is not improved. Tables 2b to 2d shows the performance changes according to the variation of the loss weight hyperparameters. The first rows show the importance of the prior losses ( $\lambda = 0.0$  cases). In particular, the absence of area prior loss may lead the model to a trivial solution and causes a significant performance drop, as described in Sec. 3.3.

## 5. Conclusion

We propose a novel framework for open-world semantic segmentation with only image-text pairs, which mainly tackles an issue in contrastive learning based methods—the discrepancy of the alignment level in training (*i.e.*, image-text) and test (*i.e.*, region-text) time. In the framework, we incorporate the grounding process within contrastive learning, thus allowing explicit learning alignment between text and text-grounded regions (*i.e.*, segmentation result). We

	$TCL_v$	$TCL_f$	CL	VOC	Ctx	Avg.
CL			✓	69.7	22.1	45.9
$TCL_v$	✓			74.4	23.3	48.9
$TCL_f$		✓		77.0	27.5	52.2
<b>TCL</b>	✓	✓		<b>78.1</b>	<b>29.1</b>	<b>53.6</b>
CL+TCL	✓	✓	✓	76.2	<b>29.5</b>	52.8

(a) **TCL loss improves performance remarkably.**

$\lambda_{TCL}$	VOC	Ctx	$\lambda_{area}$	VOC	Ctx	$\lambda_{tv}$	VOC	Ctx
0.0	-	-	0.0	68.0	28.4	0.0	74.5	28.7
0.01	75.8	22.2	0.04	70.6	<b>29.2</b>	0.1	76.0	28.6
<b>0.1</b>	<b>78.1</b>	<b>29.1</b>	<b>0.4</b>	<b>78.1</b>	29.1	<b>1.0</b>	<b>78.1</b>	29.1
1.0	68.4	28.2	4.0	75.5	22.3	10.0	71.6	<b>29.8</b>

(b)  $\mathcal{L}_{TCL}$

(c)  $\mathcal{L}_{area}$

(d)  $\mathcal{L}_{tv}$

Table 2. **Ablation studies on TCL losses and hyperparameters.** We use a short learning schedule for this ablation and refinement techniques are not applied to reveal the effect of each loss function clearly. The gray rows indicate the selected hyperparameters for our final model. Each dataset abbreviation stands for VOC: VOC20, Ctx: Context59.

also present a unified evaluation protocol for a fair and direct comparison of existing methods. Our TCL achieves state-of-the-art zero-shot segmentation performance on all 8 datasets with large margins on the evaluation protocol. We hope that this study encourages a new research direction of explicitly learning region-text alignment for open-world semantic segmentation.



## References

- [1] Nikita Araslanov and Stefan Roth. Single-stage semantic segmentation from image labels. In *Proceedings of the IEEE/CVF Conference on Computer Vision and Pattern Recognition*, 2020. 6
- [2] Minwoo Byeon, Beomhee Park, Haecheon Kim, Sungjun Lee, Woonhyuk Baek, and Saehoon Kim. Coyo-700m: Image-text pair dataset, 2022. 2
- [3] Holger Caesar, Jasper Uijlings, and Vittorio Ferrari. Cocomstuff: Thing and stuff classes in context. In *Proceedings of the IEEE conference on computer vision and pattern recognition*, 2018. 6, 13
- [4] Junbum Cha, Kyungjae Lee, Sungrae Park, and Sanghyuk Chun. Domain generalization by mutual-information regularization with pre-trained models. *European Conference on Computer Vision (ECCV)*, 2022. 11
- [5] Soravit Changpinyo, Piyush Sharma, Nan Ding, and Radu Soricut. Conceptual 12m: Pushing web-scale image-text pre-training to recognize long-tail visual concepts. In *Proceedings of the IEEE/CVF Conference on Computer Vision and Pattern Recognition*, 2021. 2, 6
- [6] Bowen Cheng, Alex Schwing, and Alexander Kirillov. Per-pixel classification is not all you need for semantic segmentation. *Advances in Neural Information Processing Systems*, 34:17864–17875, 2021. 14
- [7] François Chollet. Xception: Deep learning with depthwise separable convolutions. In *Proceedings of the IEEE conference on computer vision and pattern recognition*, pages 1251–1258, 2017. 12
- [8] MMSegmentation Contributors. MMSegmentation: Openmmlab semantic segmentation toolbox and benchmark. <https://github.com/open-mmlab/mms Segmentation>, 2020. 6
- [9] Marius Cordts, Mohamed Omran, Sebastian Ramos, Timo Rehfeld, Markus Enzweiler, Rodrigo Benenson, Uwe Franke, Stefan Roth, and Bernt Schiele. The cityscapes dataset for semantic urban scene understanding. In *Proceedings of the IEEE conference on computer vision and pattern recognition*, pages 3213–3223, 2016. 6
- [10] Mark Everingham, Luc Van Gool, Christopher KI Williams, John Winn, and Andrew Zisserman. The pascal visual object classes (voc) challenge. *International journal of computer vision*, 88(2):303–338, 2010. 6
- [11] Golnaz Ghiasi, Xiuye Gu, Yin Cui, and Tsung-Yi Lin. Scaling open-vocabulary image segmentation with image-level labels. In *European Conference on Computer Vision*, pages 540–557. Springer, 2022. 1, 2, 3
- [12] Ross Girshick. Fast r-cnn. In *Proceedings of the IEEE international conference on computer vision*, pages 1440–1448, 2015. 5
- [13] Xiuye Gu, Tsung-Yi Lin, Weicheng Kuo, and Yin Cui. Open-vocabulary object detection via vision and language knowledge distillation. *ICLR*, 2022. 2
- [14] Jack Hessel, Ari Holtzman, Maxwell Forbes, Ronan Le Bras, and Yejin Choi. Clipscore: A reference-free evaluation metric for image captioning. *EMNLP*, 2021. 2
- [15] Eric Jang, Shixiang Gu, and Ben Poole. Categorical reparameterization with gumbel-softmax. In *International Conference on Learning Representations*, 2017. 4
- [16] Aishwarya Kamath, Mannat Singh, Yann LeCun, Gabriel Synnaeve, Ishan Misra, and Nicolas Carion. Mdetr-modulated detection for end-to-end multi-modal understanding. In *Proceedings of the IEEE/CVF International Conference on Computer Vision*, pages 1780–1790, 2021. 3
- [17] Philipp Krähenbühl and Vladlen Koltun. Efficient inference in fully connected crfs with gaussian edge potentials. *Advances in neural information processing systems*, 24, 2011. 6
- [18] Boyi Li, Kilian Q Weinberger, Serge Belongie, Vladlen Koltun, and Rene Ranftl. Language-driven semantic segmentation. In *International Conference on Learning Representations*, 2021. 1, 2
- [19] Feng Liang, Bichen Wu, Xiaoliang Dai, Kunpeng Li, Yinan Zhao, Hang Zhang, Peizhao Zhang, Peter Vajda, and Diana Marculescu. Open-vocabulary semantic segmentation with mask-adapted clip. *arXiv preprint arXiv:2210.04150*, 2022. 1, 2
- [20] Quande Liu, Youpeng Wen, Jianhua Han, Chunjing Xu, Hang Xu, and Xiaodan Liang. Open-world semantic segmentation via contrasting and clustering vision-language embedding. *European Conference on Computer Vision (ECCV)*, 2022. 1, 2, 3, 5, 11
- [21] Ilya Loshchilov and Frank Hutter. Decoupled weight decay regularization. In *International Conference on Learning Representations*, 2018. 6
- [22] Roozbeh Mottaghi, Xianjie Chen, Xiaobai Liu, Nam-Gyu Cho, Seong-Whan Lee, Sanja Fidler, Raquel Urtasun, and Alan Yuille. The role of context for object detection and semantic segmentation in the wild. *CVPR*, 2014. 6
- [23] Aaron van den Oord, Yazhe Li, and Oriol Vinyals. Representation learning with contrastive predictive coding. *arXiv preprint arXiv:1807.03748*, 2018. 3, 5
- [24] Alec Radford, Jong Wook Kim, Chris Hallacy, Aditya Ramesh, Gabriel Goh, Sandhini Agarwal, Girish Sastry, Amanda Askell, Pamela Mishkin, Jack Clark, et al. Learning transferable visual models from natural language supervision. In *International Conference on Machine Learning*, pages 8748–8763. PMLR, 2021. 1, 2, 3, 4, 5, 7, 8, 11
- [25] Leonid I Rudin, Stanley Osher, and Emad Fatemi. Nonlinear total variation based noise removal algorithms. *Physica D: nonlinear phenomena*, 60(1-4):259–268, 1992. 5
- [26] Olga Russakovsky, Jia Deng, Hao Su, Jonathan Krause, Sanjeev Satheesh, Sean Ma, Zhiheng Huang, Andrej Karpathy, Aditya Khosla, Michael Bernstein, et al. Imagenet large scale visual recognition challenge. *International journal of computer vision*, 115(3):211–252, 2015. 12
- [27] Christoph Schuhmann, Richard Vencu, Romain Beaumont, Robert Kaczmarczyk, Clayton Mullis, Aarush Katta, Theo Coombes, Jenia Jitsev, and Aran Komatsuzaki. Laion-400m: Open dataset of clip-filtered 400 million image-text pairs. *arXiv preprint arXiv:2111.02114*, 2021. 2
- [28] Piyush Sharma, Nan Ding, Sebastian Goodman, and Radu Soricut. Conceptual captions: A cleaned, hypernymed, im-

- age alt-text dataset for automatic image captioning. In *Proceedings of ACL*, 2018. 2, 5, 6
- [29] Gyungin Shin, Weidi Xie, and Samuel Albanie. Reco: Retrieve and co-segment for zero-shot transfer. *Advances in Neural Information Processing Systems*, 2022. 1, 2, 3, 5, 6, 7, 11, 12, 14
- [30] Enze Xie, Wenhai Wang, Zhiding Yu, Anima Anandkumar, Jose M Alvarez, and Ping Luo. Segformer: Simple and efficient design for semantic segmentation with transformers. *Advances in Neural Information Processing Systems*, 34, 2021. 14
- [31] Jiarui Xu, Shalini De Mello, Sifei Liu, Wonmin Byeon, Thomas Breuel, Jan Kautz, and Xiaolong Wang. Groupvit: Semantic segmentation emerges from text supervision. In *Proceedings of the IEEE/CVF Conference on Computer Vision and Pattern Recognition*, 2022. 1, 2, 3, 5, 6, 7, 11, 12, 14
- [32] Yiwu Zhong, Jianwei Yang, Pengchuan Zhang, Chunyuan Li, Noel Codella, Liunian Harold Li, Luwei Zhou, Xiyang Dai, Lu Yuan, Yin Li, and Jianfeng Gao. Regionclip: Region-based language-image pretraining. *CVPR*, 2022. 2, 3
- [33] Bolei Zhou, Hang Zhao, Xavier Puig, Tete Xiao, Sanja Fidler, Adela Barriuso, and Antonio Torralba. Semantic understanding of scenes through the ade20k dataset. *International Journal of Computer Vision*, 127(3):302–321, 2019. 6, 13
- [34] Chong Zhou, Chen Change Loy, and Bo Dai. Extract free dense labels from clip. *European Conference on Computer Vision (ECCV)*, 2022. 1, 2, 3, 5, 6, 7, 11, 12, 14

## A. Architecture Details

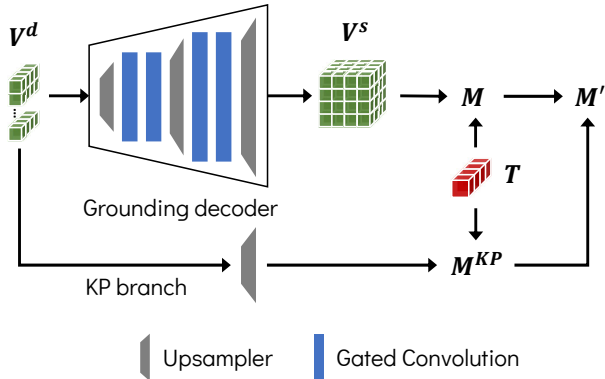


Figure 6. **Architecture of the grounding decoder.** The knowledge preservation (KP) branch serves to preserve pre-trained knowledge intact.

Our core design principle is to preserve and exploit the diverse knowledge of pre-trained CLIP [24]. Therefore, we freeze the pre-trained CLIP encoders<sup>2</sup> and train the grounding decoder for the adaptation from the image-text alignment to the region-text alignment. We also considered the other techniques to preserve knowledge [4], but a simple freezing strategy worked the best. We follow the simple modification of MaskCLIP [34] to the CLIP image encoder. They modify the last attention of the CLIP image encoder to acquire the dense features representing local semantics. These dense image features  $\mathbf{V}^d$  are fed to the grounding decoder. As shown in Fig. 6, the grounding decoder consists of four gated convolution blocks, where the output of a convolution is gated by a learned gating parameter and added to the skip connection. Concretely, the process of gated convolution can be written as:

$$\mathbf{x}' = \mathbf{x} + \tanh(g) \cdot \text{Conv}(\mathbf{x}), \quad (14)$$

where  $\mathbf{x}$  is input feature and  $g$  is a learned gating parameter. The upsamplers increase the feature map resolution for the high-resolution segmentation capability. The first two upsamplers use the nearest neighbor interpolation and the last upsampler adapts the resulting embedding into the pixel-level embedding by the bilinear interpolation. In addition, as shown in Fig. 6, we employ two branches strategy: the main grounding decoder and knowledge preservation (KP) branches. In this KP branch, the CLIP dense features  $\mathbf{V}^d$  are reshaped spatially and upsampled to pixel-level resolution by bilinear interpolation, and then we compute the text-grounded mask  $\mathbf{M}^{\text{KP}}$  by Eq. (5). There are no learnable parameters in this branch and the output masks are just

<sup>2</sup>After 30,000 iterations, we unfreeze only the last block of the image encoder for richer model capability.

	VOC20	Context59	Stuff	Avg.
ViL-Seg [20]	34.4	16.3	16.4	22.4
ReCo [29]	57.9	32.0	18.4	36.1
GroupViT (RedCaps) [31]	79.0	49.2	16.1	48.1
MaskCLIP [34]	73.0	56.5	21.9	50.5
TCL (Ours)	<b>84.5</b>	<b>62.0</b>	<b>27.6</b>	<b>58.0</b>

Table 3. **Zero-shot segmentation performance for partial classes.** The numbers of ViL-Seg are adopted from the original paper [20]. We use the proposed unified evaluation protocol for the other results.

mixed with the output from the grounding decoder branch as follows:

$$\mathbf{M}' = (1 - w_{kp}) \cdot \mathbf{M} + w_{kp} \cdot \mathbf{M}^{\text{KP}}, \quad (15)$$

where  $\mathbf{M}^{\text{KP}}$  is the generated masks from knowledge preservation branch,  $\mathbf{M}'$  is the final output mask, and  $w_{kp}$  is a mixing hyperparameter. We use the  $w_{kp}$  of 0.3. To fully leverage the massive pre-trained knowledge of CLIP [24], this branch is only used in the inference stage. It also can be regarded as a cost-free ensemble.

## B. Pseudo Code

For clarity, we provide pseudo code for the core implementation of TCL in Fig. 7. As described in Sec. 3, we first estimate the text-grounded masks via grounder, then compute the image-level and feature-level TCL losses using the masks.

## C. Additional Comparisons and Details

**Details on the comparison methods.** In the quantitative evaluation, we include the variants of the comparison baselines for an extensive comparison; the GroupViT variants from the YFCC and RedCaps checkpoints [31] and the MaskCLIP variants by the refinement process (key smoothing and prompt denoising). For the backbone of MaskCLIP, we use ViT-B/16 since its reported performance is better than ResNet-50 [34]. For the qualitative comparison, we choose the quantitatively best variant for each method.

**Comparisons with zero-shot semantic segmentation methods.** We provide an extensive and unified comparison in Table 1, but the comparison does not include non-open-sourced methods. To the best of our knowledge, ViL-Seg [20] is the only non-open-sourced method for open-world semantic segmentation. We compare the zero-shot segmentation performance following the evaluation protocol of ViL-Seg. In this evaluation protocol for zero-shot semantic segmentation, only partial classes are used: 5 classes

---

```

1 # x_t[B, L]           - minibatch of texts
2 # x_v[B, 3, H, W]    - minibatch of images
3 # text_enc           - encode text (x_t) to text emb (t)
4 # image_enc          - encode image (x_v) to global image emb (v_g) and dense feature (v_d)
5 # grounding_dec      - decode dense feature (v_d) to pixel-level dense image emb (v_s)
6 # proj               - scalar projection and sigmoid layer
7 # gumbel_max         - Gumbel-Max function
8
9 t = text_enc(x_t)    # t[B, C]
10 _, v_d = image_enc(x_v) # v_d[B, L, C]
11 v_s = grounding_dec(v_d) # v_s[B, C, H, W]
12 mask = proj(einsum("ichw,jc->ijhw", v_s, t)) # [B, B, H, W]
13
14 pos_mask = mask[arange(B), arange(B)].unsqueeze(1) # [B, 1, H, W]
15 pos_mask_b = gumbel_max(pos_mask) # binarized positive mask
16 v_g, _ = image_enc(pos_mask_b * x_v) # v_g[B, C]
17 s = v_g @ t.T # s[B, B]
18 tcl_v = info_nce(s) # InfoNCE loss
19
20 w = mask / mask.sum((2, 3), keepdim=True)
21 grounded_emb = einsum("ichw,ijhw->ijc", v_s, w)
22 s = einsum("ijc,jc->ij", grounded_emb, t) # s[B, B]
23 tcl_f = info_nce(s) # InfoNCE loss
24
25 tcl_loss = tcl_v + tcl_f

```

---

Figure 7. PyTorch-like pseudo code for the core implementation of TCL.

	TCL	GroupViT	MaskCLIP	ReCo
Speed (s)	0.20	0.17	0.16	10.60
Throughput (it/s)	4.96	5.76	6.15	0.09

Table 4. Inference speeds and throughputs.

(potted plant, sheep, sofa, train, tv-monitor) for PASCAL VOC20, 4 classes (cow, motorbike, sofa, cat) for PASCAL Context59, and 15 classes (frisbee, skateboard, cardboard, carrot, scissors, suitcase, giraffe, cow, road, wall concrete, tree, grass, river, clouds, playingfield) for the COCO-Stuff dataset. Therefore, we additionally provide the comparison results under the partial classes protocol. As shown in Table 3, TCL achieves state-of-the-art performance with a large margin in every dataset again.

## D. Inference Throughput

Open-world semantic segmentation models generally contain additional post-processing in addition to the neural network inference. For example, GroupViT [31] extracts attention maps to get the grouped regions, and MaskCLIP [34] has the refinement processes such as key smoothing and prompt denoising. Thus, we compare the methods by inference throughput instead of the number of parameters or FLOPs to examine the entire performance. We benchmark the inference speeds and throughputs using  $448 \times 448$  images and 21 target classes on a single NVIDIA V100 GPU. Benchmark setting follows an open-world scenario

that addresses an arbitrary class, *i.e.*, the text embeddings are computed for every inference. As shown in Table 4, MaskCLIP [34] is the fastest method, thanks to its low-resolution segmentation masks. It generates the segmentation masks in patch-level resolution and simply applies bilinear upsampling to achieve pixel-level resolution. It is originally a drawback of the method, but it helps with inference throughput. ReCo [29] shows very low throughput due to its retrieval process; it retrieves similar images from the ImageNet dataset [26] and co-segments the images. TCL is slightly slower than GroupViT and MaskCLIP, because TCL generates high-resolution segmentation maps, which requires a relatively large computational cost. Note that there is a lot of room to reduce the computational cost, *e.g.*, utilizing depthwise convolution instead of standard convolution [7], but it is not the focus of this study; we leave it to future work.

## E. Case Study on Failures

**Errors of TCL.** We investigate the failure cases of TCL via various qualitative examples. First, TCL undergoes difficulty in capturing segment boundaries accurately. For example, in Fig. 8b, the predicted segment of the “mountain” class includes part of the sky region, and the “cell phone” segment contains the right hand and arm regions. This is a fundamental challenge of unsupervised open-world segmentation; the absence of dense annotation makes precisely capturing a segment boundary extremely difficult. Although the proposed method remarkably improves the segmenta-



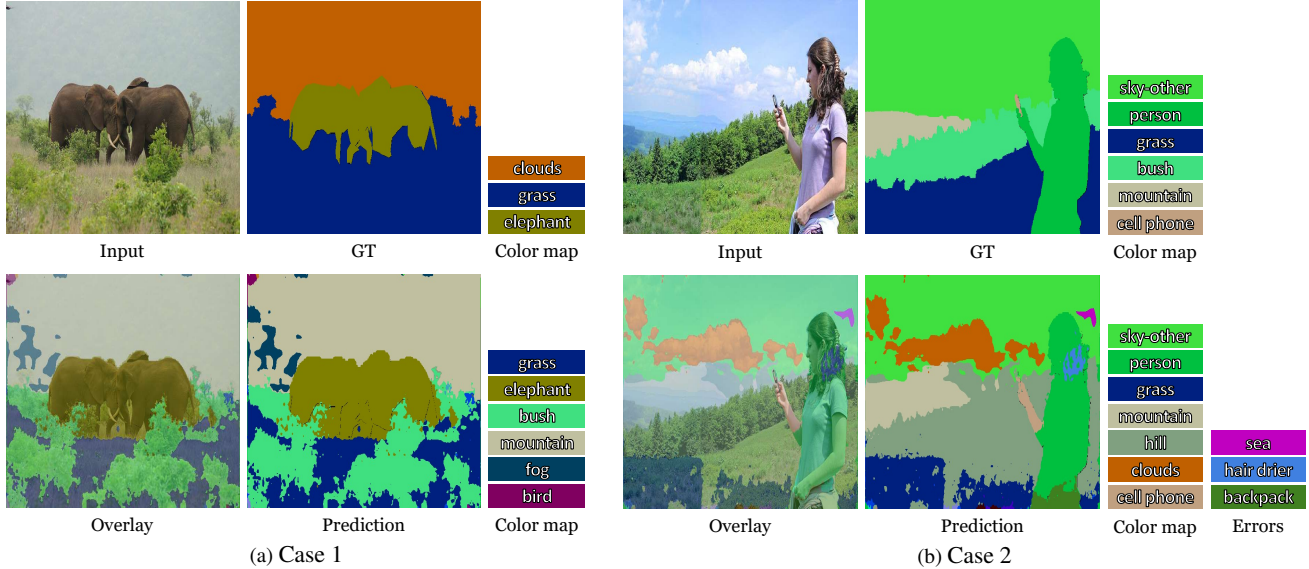


Figure 8. **Ambiguous error cases.** The color map of a negligible region is omitted. Although different from the ground truth (GT), there are many cases that can be considered correct. The segments in the color map are semantically correct despite of difference with GT, while the errors indicate clearly incorrect predictions.

tion performance compared with previous methods, this case study reveals that there are still many areas to be improved. Furthermore, despite the help of the smooth prior loss, the predictions still tend to be noisy, *e.g.*, “sea” or “hair drier” in Fig. 8b.

**Ambiguity in benchmarks.** On the other hand, we also find crucial issues in the current benchmark datasets: ambiguities in the class label set and scene semantics. In particular, there are lots of class labels with similar semantics, especially in the datasets with a large vocabulary, *e.g.*, COCO-Stuff (171 classes) [3] or ADE20K (150 classes) [33]. Mostly the labels have different semantics in detail, but the distinction between the labels can be ambiguous depending on how the image captures the scene. For example, it is hard to distinguish “clouds” and “fog” in Fig. 8a and “hill” and “mountain” in Fig. 8b. Also, there are labels with superset-subset relations. For instance, the COCO-Stuff dataset has “broccoli”, “vegetable”, and “food-other” classes. In the supervised setting, a model can address this issue by training only if there is labeling consistency between images. However, in the open-world scenario, such superset-subset relations cause significant ambiguity. Furthermore, a more frequent ambiguity raises when a segment has multiple semantics. More proper descriptions of the “clouds” and “grass” segments in Fig. 8a are “foggy or cloudy mountain” and “bushes on the grass”, respectively. However, ground truth (GT) labels represent only part of the entire semantics. As with the superset-subset relation case, benchmarks for the open-world scenario require ad-

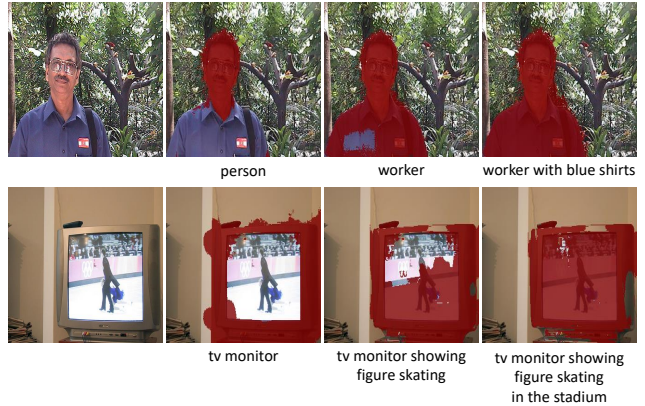


Figure 9. **TCL behaviors depending on the specificity of the prompts.** The red-colored region indicates the segmentation results of the given text prompts. The more specific the prompt, the better the segmentation result.

ditional consideration to address such ambiguities. In this study, we propose a unified evaluation protocol to compare the existing methods fairly, but it only unifies the evaluation protocol and simply employs existing benchmark datasets. This analysis suggests the need for further advanced benchmarks dedicated to open-world scenarios in the future.

## F. Analysis on Model Behavior

In this section, we investigate how the learned TCL model generates different segmentation masks depending on the input text prompts. As shown in Fig. 9, the model tends to capture the intended region better when the in-

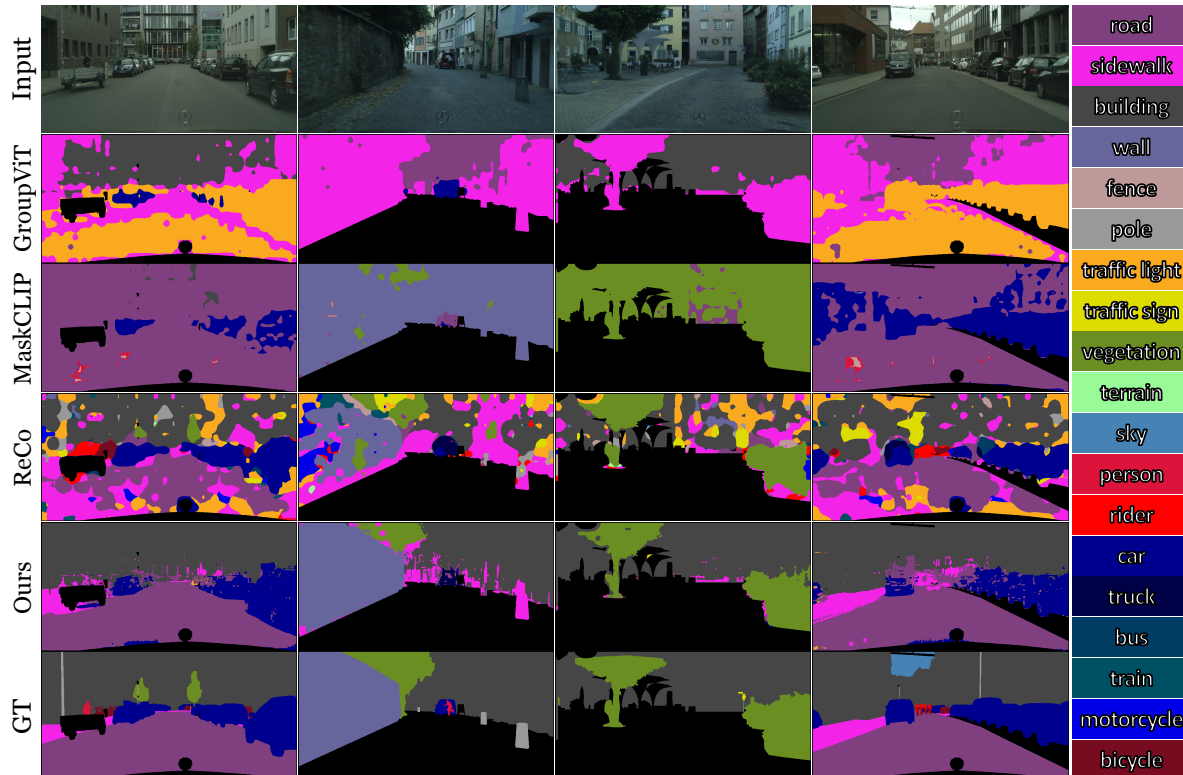


Figure 10. Additional qualitative examples on Cityscapes.

put text prompt is more specific. Although this characteristic can cause performance degradation when evaluating the model on a fixed benchmark, it also improves the controllability of the model. We can exploit this controllability to maximize the benchmark performance, *e.g.*, class name expansion. However, we do not employ these dataset-dependent tricks to prevent the overestimation of the model performance, as described in Sec. 4.1.

## G. Additional Qualitative Results

### G.1. Qualitative Examples on Complicated Scene

Qualitative comparison on PASCAL VOC in Sec. 4.3 visualizes the performance difference between comparison methods. However, the VOC dataset tends to be object-oriented and its images are generally composed of one or two segments. In this section, we qualitatively compare open-world segmentation methods in complicated scenes. Figs. 10 and 11 show examples including at least 3 segments from the Cityscapes and COCO-Stuff datasets. As shown in the figures, GroupViT [31] and MaskCLIP [34] tend to generate a small number of segments. It makes the results less noisy but causes a large error. For example, in Fig. 10, MaskCLIP fails to segment “building” regions and GroupViT misidentifies “road” as “traffic light”. In contrast, ReCo [29] suffers from noisy prediction. Our

TCL also generates partially noisy results, but it is relatively cleaner and better than the comparison baselines. It is also worth noting that the image resolution of the unified evaluation protocol is relatively smaller than the widely used protocols for Cityscapes. We resize a shorter side of an image to 448 with keeping the aspect ratio, resulting in  $448 \times 896$ . In contrast,  $1024 \times 2048$  is the widely used resolution for the Cityscapes dataset [6, 30]. Increasing the resolution can help recognize small objects, *e.g.*, the persons in Fig. 10.

### G.2. Additional Qualitative Examples in the Wild

Fig. 12 shows additional qualitative examples from web images in the wild. In this experiment, we investigate the discrimination capability of the model in various aspects: proper nouns (Frodo, Gandalf, Pyramid, Sphinx, Samwise, Gollum, Taj Mahal, Batman, Superman), colors with the same object (red, green, yellow bananas), letters (MMU, Turkish, Fighter), and subclasses (Corgi, Shepherd). The results show that our model can recognize and segment various concepts in the wild. For the baseline models, the results show similar tendencies with the in-the-wild examples in Sec. 4.3. Contrary to the quantitative evaluation in fixed benchmarks, ReCo [29] generates a relatively plausible segmentation map compared with GroupViT [31] and MaskCLIP [34].



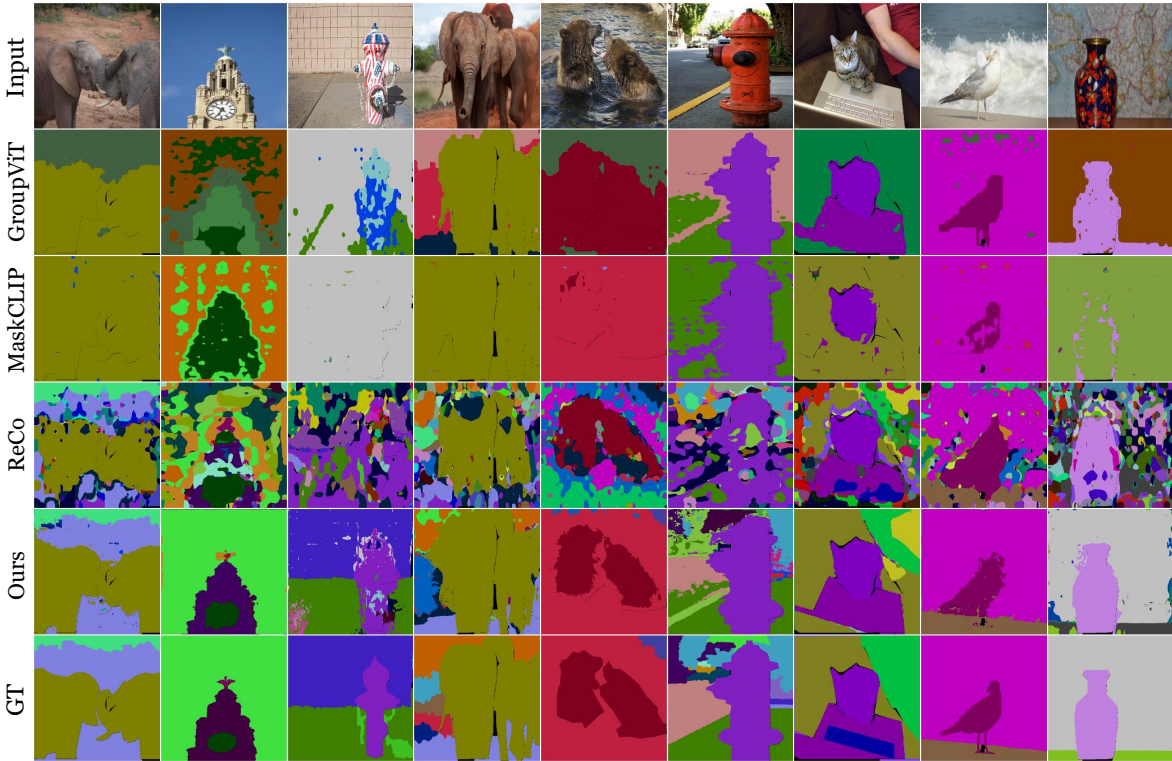


Figure 11. Additional qualitative examples on COCO-Stuff. Color map is omitted since COCO-Stuff has 171 classes.



Figure 12. Additional qualitative examples in the wild.